Reprinted without change of pagination from the
Journal of Fluid Mechanics, *volume* 18, *part* 2, *pp.* 285–301, 1964

Experiments on jet flows and jet noise far-field spectra and directivity patterns

By ERIK MOLLO-CHRISTENSEN, MARC A. KOLPIN AND JOHN R. MARTUCCELLI

Massachusetts Institute of Technology, Cambridge, Mass.

(Received 26 March 1963 and in revised form 8 August 1963)

The results of measurements of far-field sound emitted from jets are reported. The narrow-band power spectral density of the sound in the far field was measured for three jet diameters, three Mach numbers, and five angular positions. The intensity distribution of mean-square pressure fluctuation in the far field in several wide frequency ranges were also measured. The similarity relations found from the experiments are reported.

1. Introduction

The problem of jet noise is still of technological interest. In addition, it is of interest as a problem in fluid dynamics in the class of problems which involve the interaction between instability, turbulence and wave emission. Other problems of this class are found in meteorology, oceanography and astrophysics.

Our present understanding of jet noise may be sufficient for *ad hoc* applications in aeronautics, and present methods of noise suppression may be acceptable (Lighthill 1961). The problem does, however, remain of interest in the field of fluid mechanics.

Previous experiments on jet noise have been insufficiently precise for assessment of the validity or relative merit of proposed theories. Very little data exists, for example, on the noise emission from jets where both the mean flow field and the turbulent field are known. One is in the situation where more is known about the emitted sound than is known about the structure of the emitter.

A theory of a stochastic field can only be proved by experiment either by showing that all the assumptions are valid or by showing that the theory correctly predicts all the joint statistical measures of the field. A theory which yields a good approximation to only a few of the structural measures, such as mean-square fluctuations and spectral densities for a restricted parameter range, need not be physically correct in detail in order to be useful.

The purpose of the present experiments on jet noise and jet flows was to obtain more precise and detailed information about the flow field and the sound emission. Extensive precautions were therefore taken in the design of the experimental apparatus to insure controlled circumstances. The specific information sought was on the dependence and interdependence of the flow field and the emitted sound. The turbulent velocity field in a jet is in part universal, in part determined by the exit conditions. The relative importance of the universal and the peculiar

parts of the turbulent field as sound emitters were sought. The jet formed by a fully developed turbulent pipe flow beyond the pipe termination may, for example, emit sound which is characterized by the transition from pipe-flow turbulence to fully developed jet turbulence, while a laminar but unstable jet may emit sound of a single frequency. It is also possible that in some cases the process of sound emission cannot be separated from the mechanism of generation of turbulence. An example is found in so-called sensitive jets, which can be excited into oscillation by an impinging sound field, and which will amplify the sound. If one has two adjacent sensitive jets, they may excite one another. Clearly, in such a case, it is not possible to ignore the effect of sound upon the mechanism of generation of turbulence. However, even in this case, the sound field can be described in terms of the velocity fluctuations, using, for example, Lighthill's (1954) theory. Before one can apply such a theory, however, the velocity field must be known.

2. Experimental arrangement

The apparatus used in the experiments consisted of a flow-producing apparatus, an anechoic chamber, sensing elements and data-processing equipment. These elements and their characteristics will be described to the extent that is directly relevant to the measurements of far-field sound. Other characteristics will be mentioned in their proper context in reports on other measurements.

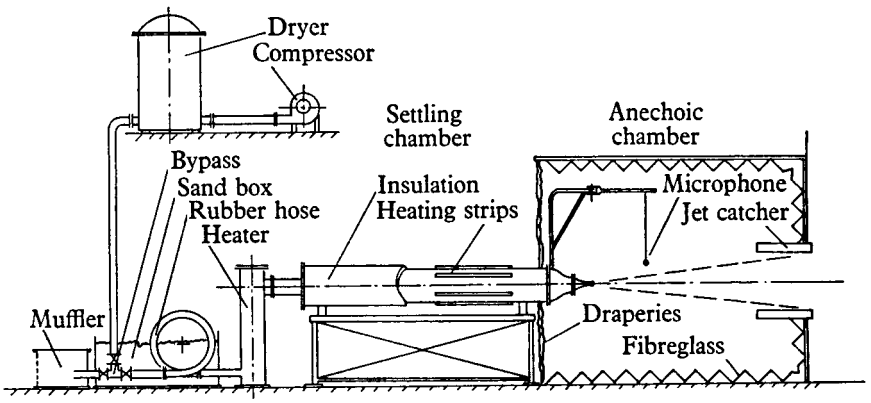

FIGURE 1. Flow-producing apparatus.

2.1. *Flow-producing apparatus*

Figure 1 shows the flow apparatus. Dry, compressed air enters a muffler-settling chamber after having passed through a heater. The air leaves the settling chamber through a contraction, ending in a nozzle. Three nozzles of different exit diameters but geometrically similar in shape were used. Figure 2 shows the 1 in. nozzle. The nozzle exit is in the anechoic chamber. The air leaves the chamber through a 'jet catcher' as shown in figure 1.

The settling chamber, made of a heavy cast-iron pipe, had a diameter of 12 in. and was 10 ft. long. In the first 2 ft. of the settling chamber high turbulent mixing was generated so as to equalize the velocity and temperature of the air

after it had passed through the heating elements. The next 6 ft. were used to reduce the turbulence level. This was done by five sections of steel wool, each 6 in. thick, held between screens. The flow was then straightened by a honeycomb, 1 ft. long, made of finned steel tubing. Preceding the 18 in. stilling section were three screens of decreasing mesh size. The jet nozzles were fastened at the end of the pipe. As a result of more than 1 year spent in eliminating extraneous

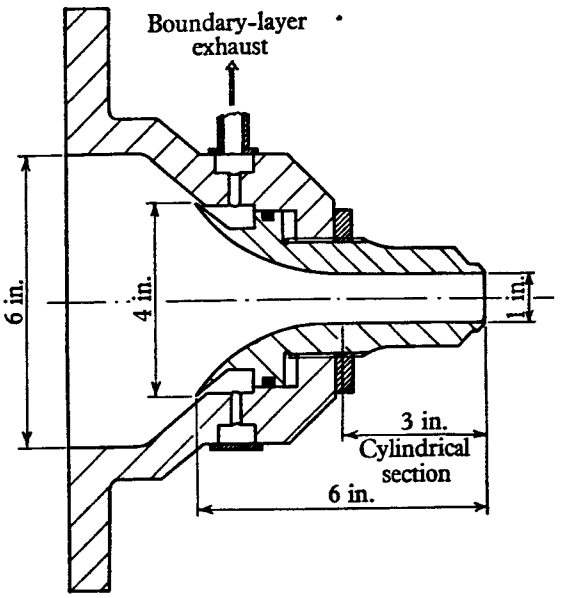

FIGURE 2. The 1 in. nozzle.

sources of sound and turbulence, the system now gives a flow with an r.m.s. turbulent velocity level which cannot be detected using a Shapiro and Edwards hot-wire set and tungsten wires of a diameter of 10^{-4} in., no detectable temperature fluctuations, very little sound from sources upsteam of the nozzle exit, and no detectable effects of nozzle vibration.

2.2. *Anechoic chamber*

The $8 \times 8 \times 8$ ft. chamber was designed for short wavelengths of sound. The walls, ceiling and floor are covered by two layers of 1 in. thick fibreglass mats with the outer layer wavy, as shown in figure 1. The upstream wall, on which little sound will impinge, is a curtain of heavy cloth.

2.3. *The microphone*

A Bruel and Kjaer condenser microphone was used for all the far-field measurements. Its face diameter is $\frac{1}{2}$ in., its frequency response flat for axially impinging sound from 20 to 35,000 c/s. The r.m.s. signal-to-noise ratio was below 5×10^{-3} in all the runs. The microphone was periodically calibrated using the 'piston phone' supplied by the manufacturer. The sensitity was found to remain constant ($s = 1{\cdot}03 \times 10^{-3}$ V/μbar).

The microphone was supported by a horizontal boom which could rotate about a vertical axis through the centre of the nozzle exit plane. The microphone was hung from the boom using loosely spun cotton twine. The maximum inaccuracy in microphone position was $\frac{1}{10}$ in.

2.4. *Data processing system*

For the far-field sound measurements, the system shown in figure 3 was used. As the figure shows, the power spectrum recorder consisted of a Donner (model no. 2102) wave-form analyser and a Leeds and Northrup Speedomax pen recorder. The power band-pass of the wave-form analyser was found to be 25 c/s, measured

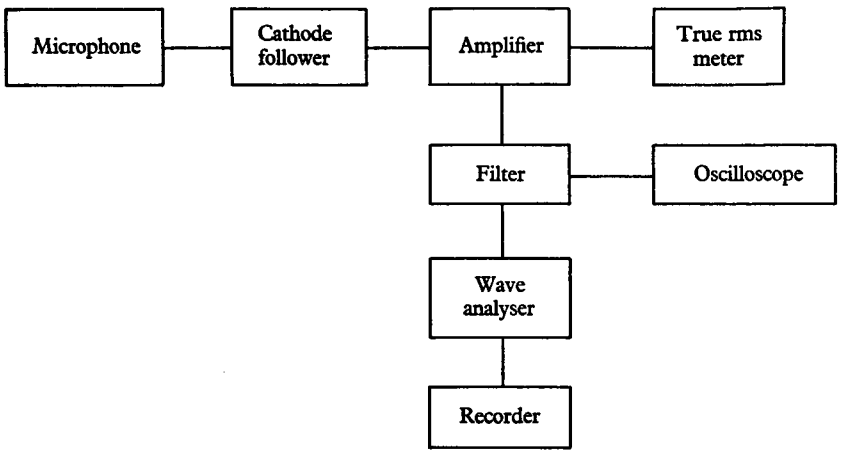

FIGURE 3. System for far-field sound measurement.

as the width of an equivalent rectangular spectral window. The paper-drive mechanism of the pen recorder was mechanically linked to the frequency dial of the wave-form analyser. The electric output of the wave-form analyser was fed to the recording pen, which plotted the square root of the power spectral density of the wave-form analyser input. A built-in calibration was used to check for accidental drift of the microphone, amplifier, analyser and recording during a run.

In addition, the r.m.s. signal from the microphone was read on a true r.m.s. meter, and a Panoramic (model SB15a) wave-form analyser was used for monitoring the complete spectrum.

3. Elimination of parasitic sources of noise and turbulence

The procedure used to identify and eliminate parasitic noise sources were based on the contention that the only physical variables of interest were those describing the nozzle geometry, the mean-flow parameters at the nozzle exit, the fluctuations in the free jet and the sound field and the microphone location. Therefore, data which do not depend upon any other variables can be stated as functional relationships of non-dimensional variables formed from the admissible physical variables. A variation of the dimensional parameters which does not

affect the values of the dimensionless quantities should not change the functional relationship between the latter.

However, if parasitic variables are present and affect the phenomenon under investigation to a discernible extent, such a variable must be included in order to state the result in terms of dimensionless variables. This is well known to experimenters, and usually it is not very difficult to design and modify an experiment in fluid dynamics so that no parasitic variables affect the results. For the experiments described in this paper, it proved difficult indeed to eliminate unwanted effects. First, a radiative phenomenon such as sound can transmit energy over large distances and focus it so that a parasitic effect can be felt far away from its source. Also, distant boundaries must neither radiate nor reflect sound. Also, the sound emission from a jet contains only a small fraction of the jet energy. A small change in the jet flow which just happens to be an efficient sound emitter can therefore upset the sound field significantly. Another difficulty was our insistence upon similarity in narrow band-pass spectra. An effect which does not show up in the mean square or even in averages over broad frequency bands may show up very well in a spectrum with sharp frequency resolution.

Among the phenomena which gave parasitic effects were: sound scattering from microphone supports and cables, unstable flow in the air outlet from the anechoic chamber and amplifier microphonics. We believe that we have eliminated all the important parasitic effects, and that our power spectral densities are correct within 10 %.

4. Experimental results

The results which will be reported in this paper consist of (1) the Mach number profiles of the mean flows, which are included here for purposes of reference, and will be further discussed in a future paper; (ii) the root-mean-square of the pressure fluctuations in the far field as a function of microphone position and the jet-flow parameters; (iii) the power-spectral densities of the far-field pressure fluctuations as functions of microphone location and jet-flow parameters.

4.1. *Mean-flow profiles*

Typical mean-flow profiles are shown in figures 4 and 5 for two jet diameters. The quantities plotted are Mach number, $M(x, y)$, *vs* $\eta = 1-(2y/D)/x$, x being the downstream distance from the nozzle exit plane and y the radial distance from the jet centre-line. The location of the jet centre-line was determined by measurement of stagnation-pressure profiles. Note the longer laminar core of the smaller jet. A complete report on the mean-flow profiles has been given by Kolpin (1962).

4.2. *Root-mean-square pressure fluctuations in the far field*

From dimensional analysis, the root-mean-square pressure fluctuation $\tilde{p}$ in the far field of a circular jet must satisfy a relation of the form

$$\frac{\tilde{p}}{K\rho a^2} = f_1(M, Re, D/r\,\theta),$$

where K is a dimensionless constant, ρ a density, a the speed of sound at the nozzle exit, M the Mach number, D the nozzle diameter, r the distance from the centre of the nozzle exit plane to the microphone, θ the angle between r and the axis of symmetry of the jet, $U = aM$, $Re = UD/\mu$ and μ is the kinematic viscosity.

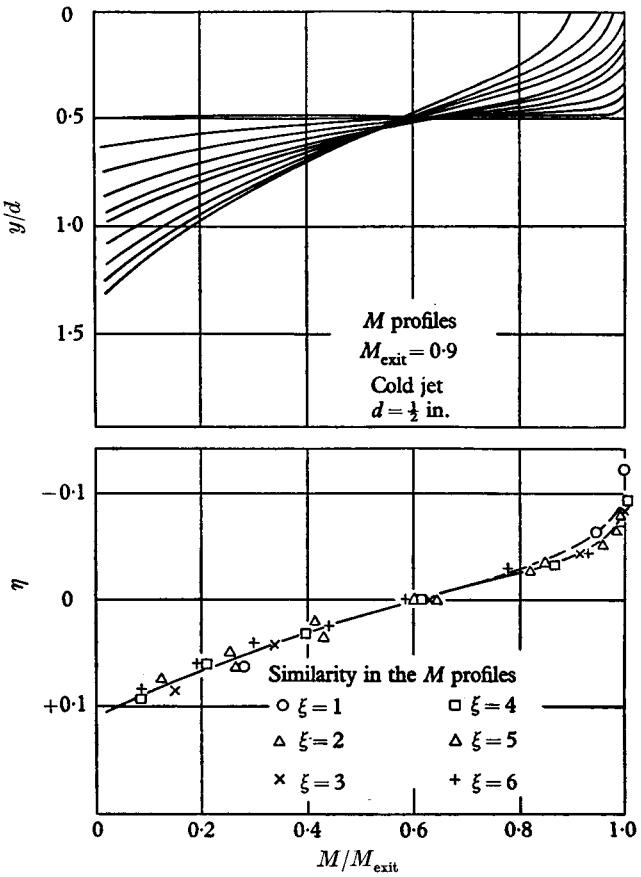

FIGURE 4. Mean flow.

Confining the attention to the far field of emitted sound, where, by definition, $\tilde{p}$ varies as the inverse of the distance, one obtains

$$\frac{\tilde{p}}{K\rho a^2} = \frac{D}{r} G(M, Re, \theta).$$

The function G has to be determined from experiments. The experiments were designed to measure the dependence of G upon M and θ directly, and to separate the dependence of G upon M and Re as far as possible by investigating the sound emission from jets of different diameters.

The data obtained satisfy the far-field relationship within a few percent for $D/r > 30$ for frequencies f above $fD/a = 10^{-2}$.

4.3. *Directivity of far-field sound*

All the data were obtained in one plane passing through the jet axis. Measurements elsewhere in the field showed that the sound field was axisymmetric within 2 % of $\tilde{p}$.

Figure 6 shows contours of constant $\tilde{p}$ in the (r, θ)-plane, for $M = 0{\cdot}8$ and $M = 0{\cdot}9$ and $D = 1$ in. The numbers marked on the contours are the r.m.s. of the signal in millivolts. Note the corrected value for $M = 0{\cdot}9$. The figure

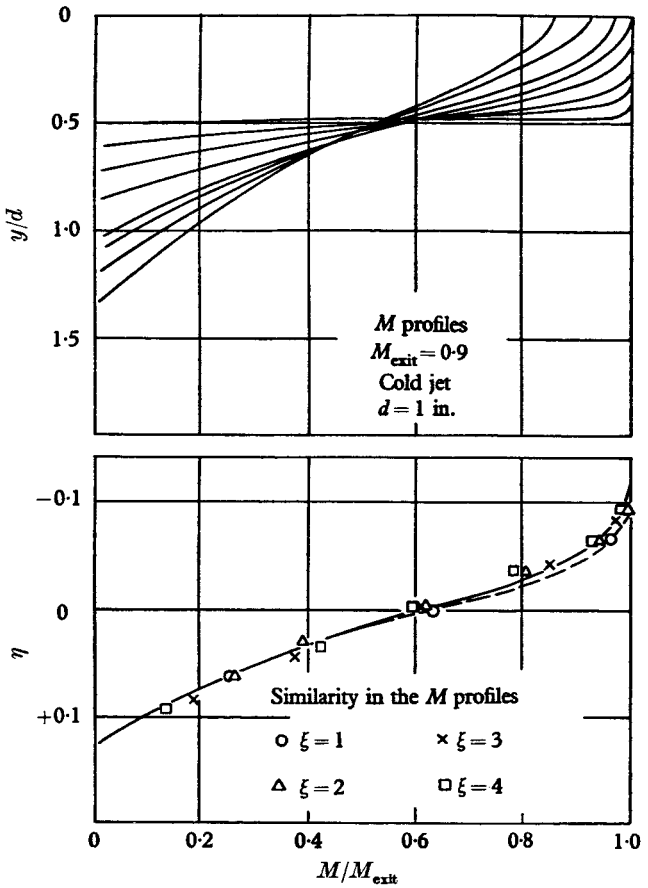

FIGURE 5. Mean flow.

shows a single lobe in the directivity pattern, and that $\tilde{p}$ is not quite proportional to M^4 as suggested by Lighthill as a first approximation, while the variation of $\tilde{p}$ with θ is almost independent of Mach number. The single lobe emission pattern is different from that obtained by previous investigators. The reason is that in our measurements low values of dimensionless frequency could be included. For large jet diameters, the lower frequencies are easily masked by the effects of gust upon the microphone, usually classified as 'pseudosound' and filtered out. The measurement of $\tilde{p}$ presented in figure 6 extends from $fD/U = 10^{-2}$ to $fD/U = 5$. This point is demonstrated in figure 7, which shows contours of constant $\tilde{p}$

when frequencies below $fD/U = 2$ have been excluded by filtering the signal. The familiar directivity of the sound field is apparent, the maximum being near $\theta = 45°$.

The corresponding distribution of low frequency emission is shown in figure 8, where only frequencies in range $0 < fD/U < 0{\cdot}5$ have been included. These low frequencies seem to be emitted most intensely within the jet itself, where measurements are very difficult, if not impossible.

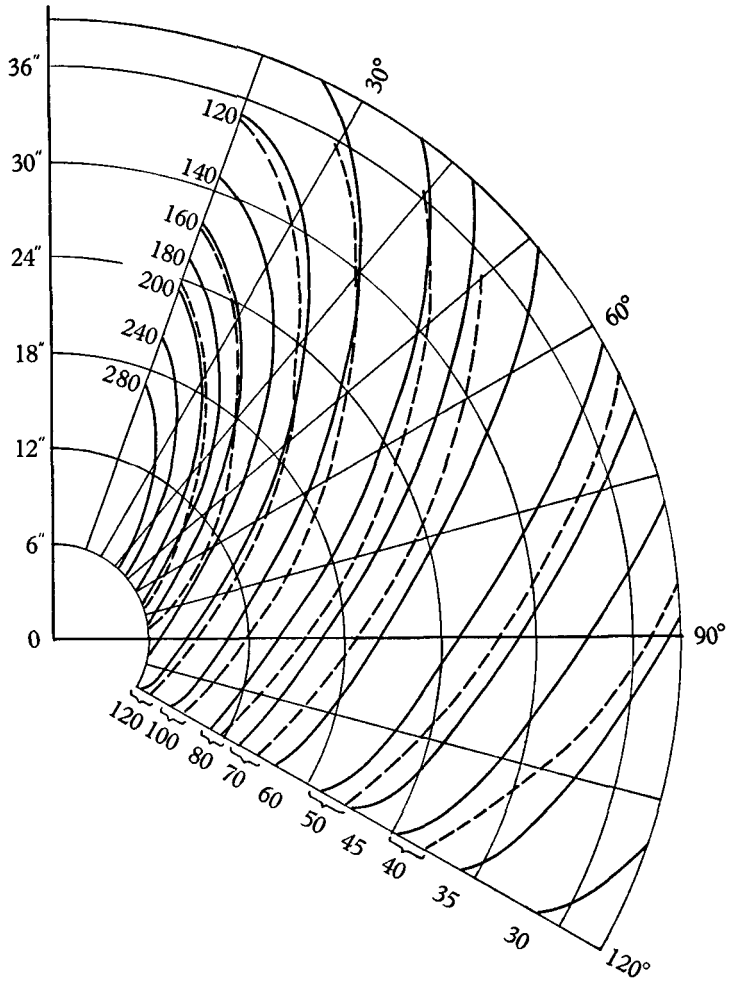

FIGURE 6. Contours of constant $\tilde{p}$ in field, jet axis at $\theta = 0°$; $M = 0{\cdot}8$ and $0{\cdot}9$; $D = 1$ in.; $\tilde{e}$ in mV, at $M = 0{\cdot}9$, $\tilde{e}$ ——. At $M = 0{\cdot}8$, $(0{\cdot}9/0{\cdot}8)^4\,\tilde{e}$ – – – –.

Figures 7 and 8 indicate that the large and the small eddies within the jet may differ in their sound production, and that one may be able to make a distinction between them as sound emitters.

The directional distribution of sound intensity appears to be almost independent of Mach number. Figure 9 gives further evidence in this direction, showing the dependence of $\tilde{p}$ upon θ for three different values of M. The curves have the

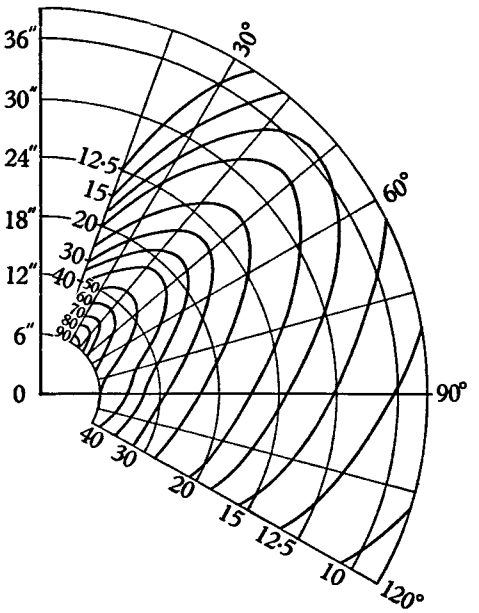

FIGURE 7. Contours of constant $\tilde{p}$ for high frequencies only. $M = 0{\cdot}8$; $D = 1$ in.; $fU/d > 2$; r.m.s. in mV.

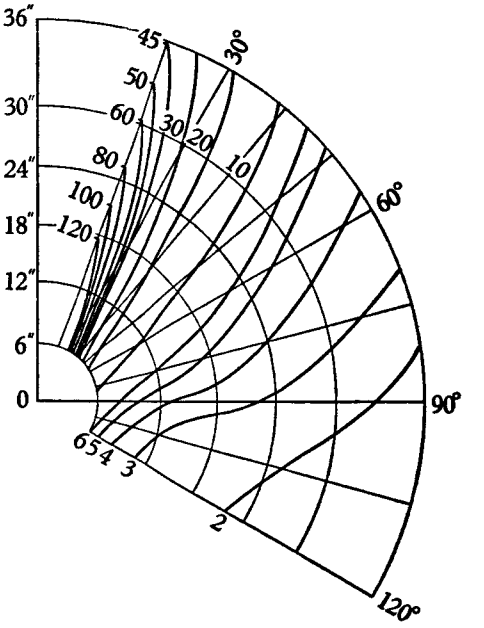

FIGURE 8. Contours of constant $\tilde{p}$ for low frequencies only. $M = 0{\cdot}8$; $D = 1$ in.; $fU/d > 0{\cdot}5$; r.m.s. in mV.

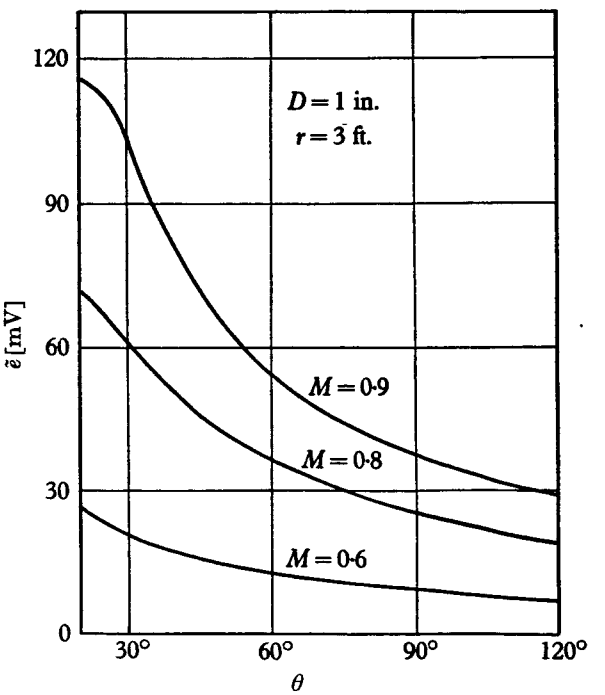

FIGURE 9. Variation of r.m.s. microphone output $\tilde{p}$ with θ and M. (Independent measurement for these shown in figure 8.)

same shape for $\theta > 40°$. The variation of $\tilde{p}$ with diameter is shown in figure 10 for $M = 0{\cdot}8$. The ordinates have been arbitrarily scaled so as to coincide for $\theta = 50°$. The correspondence is quite good, and the directivity is approximately

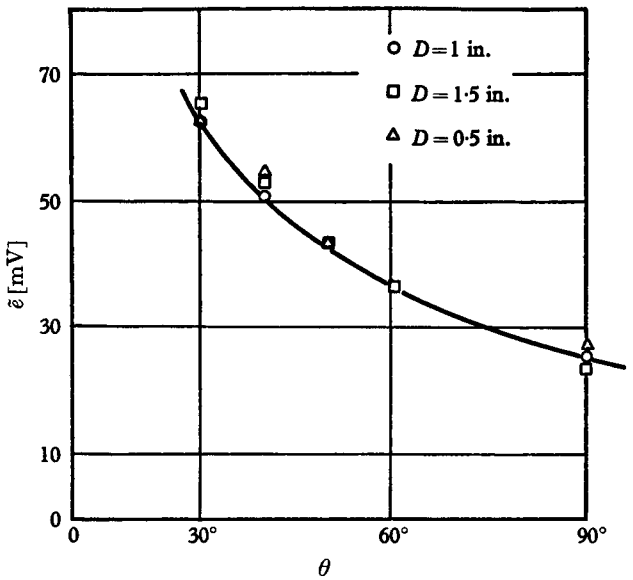

FIGURE 10. Variation of r.m.s. microphone output with jet diameter and θ for $M = 0{\cdot}8$, scaled so as to make data coincide at $\theta = 60°$.

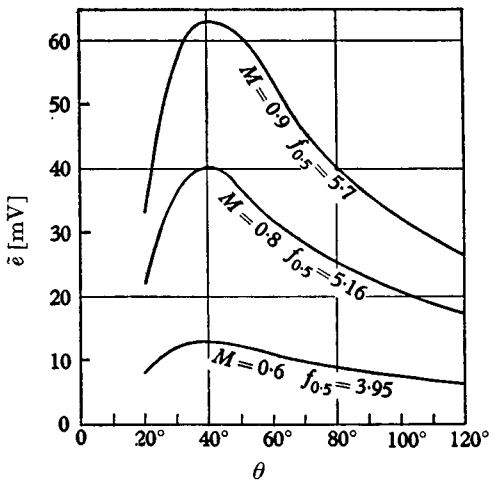

FIGURE 11. Variation of high frequency sound with θ and M for $S > 2$. $r = 3$ ft., $D = 1$ in., independent measurement; $f_{0{\cdot}5}$ is shown measured in kc/s.

independent of jet diameter for a given Mach number, but does depend strongly upon frequency and to a lesser extent upon Mach number.

The results of a separate experiment are shown in figure 11 where the mean-squares of frequencies above $fD/U = 2$ are included, lower frequencies having

been filtered out. For high frequencies, the directivity of sound emission is independent of Mach number and Reynolds number. This suggests that the function $G(M, Re, \theta)$ may conveniently be written in the form

$$G(M, Re, \theta) = F(\theta)\, M^{n(\theta)} G_1(M, Re, \theta)$$

for the high frequency portion of the sound field, where $G_1(M, Re, \theta)$ is a slowly varying function of M and θ.

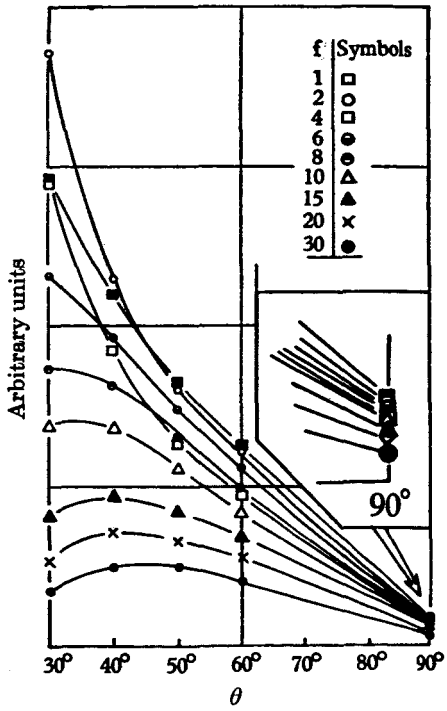

FIGURE 12. Far field $\tilde{p}$ *vs* θ at selected frequencies for $M = 0{\cdot}8$, $D = 1$ in., $r = 2$ ft. (independent experiment from other results shown in this paper). f is measured in kc/s.

A firmer indication of the dependence of directionality upon frequency is shown in figure 12 which is the result of measuring the root-mean-square of a narrow frequency band as a function of θ for a fixed M and D. The power bandwidth for these measurements was 25 c/s.

The angle of maximum intensity decreases with frequency, showing that the spectra and directivity distributions of high and low frequencies are different and there is a smooth transition between them.

4.4. *Dependence upon Mach number and Reynolds number*

To find the Mach number dependence of the mean-square intensity of sound in the far field, the results of a series of measurements of $\tilde{p}$ was plotted against M on log-log paper and the value of $n(\theta)$ determined on the presumption that

$$\frac{\tilde{p}}{K\rho a^2} = \frac{D}{r} G(M, Re, \theta) \sim M^{n(\theta)} F_2(Re).$$

A sample plot is shown in figure 13. Measurements were made for $M = 0{\cdot}6$, $0{\cdot}8$ and $0{\cdot}9$.

It was found that $n(\theta)$ is independent of M, and figure 14 shows the variation of $n(\theta)$ for three different jet diameters. $n(\theta)$ varies between 4·4 and 3·6. Lighthill suggests that the average value of $n(\theta)$ should be four, yielding $(\tilde{p})^2 \sim M^8$. This estimate appears to be high.

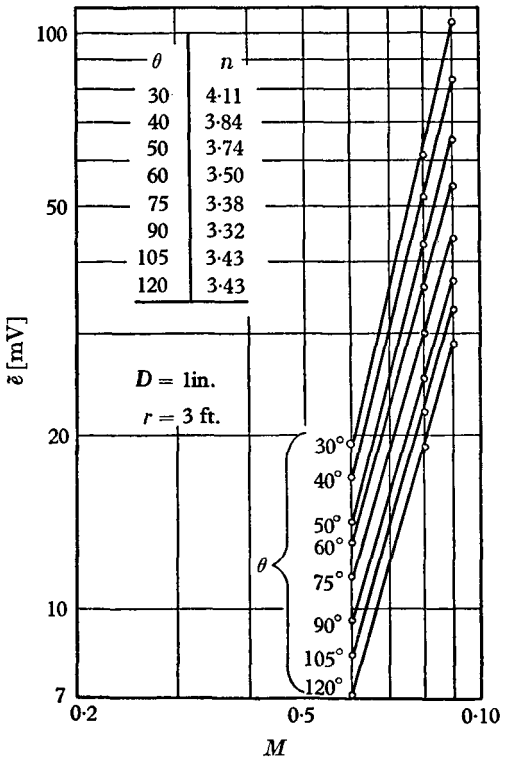

FIGURE 13. Variation of microphone output with M and θ. Independent experiment.

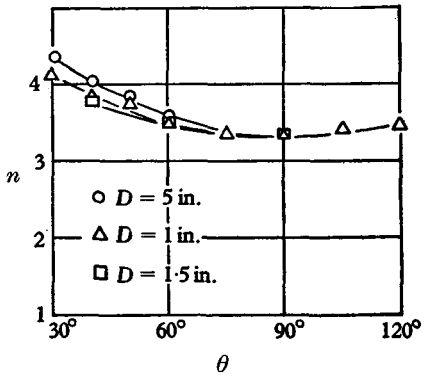

FIGURE 14. Variation in Mach number exponent with diameter D and θ for best fit of formula, $\tilde{p} \sim M^n$.

A most naïve attempt at finding the variation of $\tilde{p}$ with Reynolds number is to try an approximation of the type

$$\tilde{p} \sim Re^m = (UD/\nu)^m.$$

Taking account of the dependence upon M already found, one can then set

$$\tilde{p} \sim M^{n-m}(Re)^m.$$

The data then shows m to be between one and three, m decreasing with increasing nozzle diameter. This result is due to the fact that transition moves from the free shear layer for the smaller jet at low Mach number to the nozzle boundary layer for the larger jets and higher Mach numbers. One can only conclude from the present measurements that whether transition takes place in the free shear layer or not has an easily discernible effect upon sound emission.

5. Power spectrum measurements

The power spectral density $\Phi(f)$ and the mean square $\tilde{p}^2$ of the pressure fluctuations are related by

$$\tilde{p}^2 = \int_0^\infty \Phi(f)\,df. \tag{5.1}$$

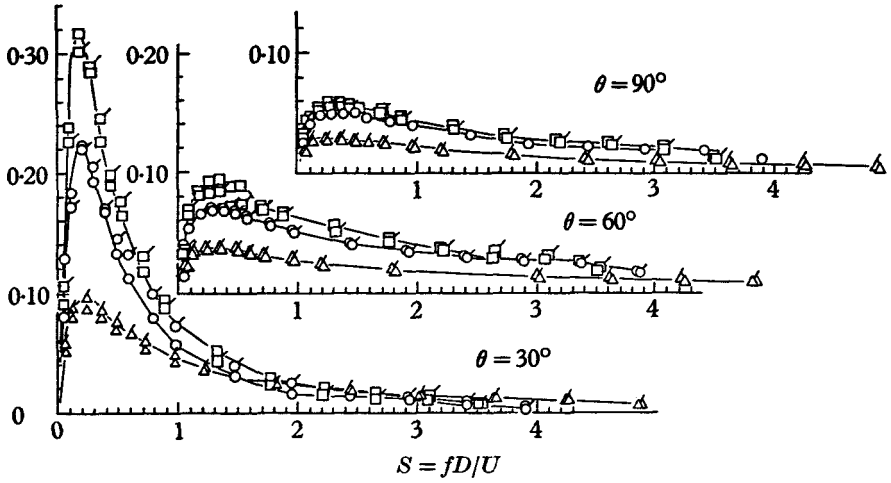

FIGURE 15. Far-field sound spectra showing departures from far-field relationships for different values of M and θ; D = 1 in. The points are shown in the following table:

R/D	θ	30°	60°	90°
24		□ M = 0·895	□ M = 0·893	□ M = 0·893
		○ M = 0·795	○ M = 0·800	
		△ M = 0·622	△ M = 0·623	△ M = 0·623
36		□ M = 0·895	□ M = 0·898	□ M = 0·898
		○ M = 0·798	○ M = 0·800	○ M = 0·785
		△ M = 0·622	△ M = 0·623	△ M = 0·623

In the far field, $\tilde{p}^2$ must vary as the inverse square of the distance r, and from dimensional considerations one finds that $\tilde{p}^2$ must be expressible in the form

$$\tilde{p}^2 = (\tfrac{1}{2}\rho a^2 M^2)^2 (D^2/r^2) \int_0^\infty \phi(S)\,d(fD/U), \tag{5.2}$$

where $\phi(S)$ is a dimensionless function of Strouhal number $S = fD/U$, and where a and N are measured in the jet at the nozzle exit.

Comparing equations (5.1) and (5.2), one finds that $\phi(S)$ and $\Phi(f)$ are related by

$$\phi(S) = \frac{\Phi(f)}{(\tfrac{1}{2}\rho a^2 M^2)^2} \left(\frac{r}{D}\right)^2 \frac{U}{D}.$$

$\phi(S)$ may be considered a dimensionless power spectral density.

Figure 15 shows a number of measured spectra, plotted as $\phi(S)$ *vs* S on linear scales. The figure is included to show the extent to which the far-field relationship holds for data obtained at different values of r/D and to give an impression of the experimental error. The spectra shown are for one jet diameter, three values of Mach number and at four angles θ between r and the jet axis.

It is, of course, rather difficult to obtain far-field similarity for small values of θ at low frequencies, since the point of observation is not far from the emitter, as measured in either wavelengths or emitter extents. Figure 15 confirms this.

Figure 16 shows thirty spectra which were obtained in the far field. The curves shown are drawn through the measured points in order to avoid excessive clutter of symbols. The maximum scatter of experimental data obtained at two distances r is less than 10 %.

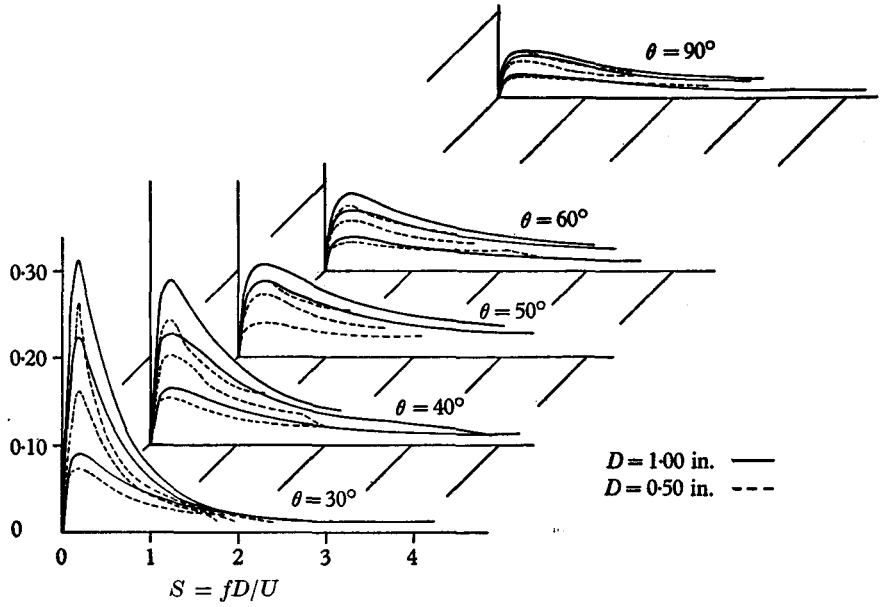

FIGURE 16. Far-field spectra for different values of M and θ for two jet diameters.

The spectra shown in figure 16 represent for three values of Mach number, $M = 0{\cdot}62$, $0{\cdot}80$ and $0{\cdot}90$, five angular positions, $\theta = 30°$, $40°$, $50°$, $60°$ and $90°$, and two jet diameters, namely $D = \frac{1}{2}$ in. and $D = 1$ in., corresponding to Reynolds numbers $Re = UD/\nu$ of approximately $3M \times 10^5$ and $6M \times 10^5$, respectively. The results show that most of the noise is emitted in the frequency range $0{\cdot}1 < S < 1{\cdot}0$. The data also show that $\phi(S) = 0$ for $S = 0$. This means that either the emitter intensity is zero at zero frequency or that the total equivalent emitter contains no simple source.

The slope of $\sqrt{\phi(S)}$ is finite and appears to be constant near $S = 0$. The constant slope portion of $\sqrt{\phi(S)}$ is less obvious at $\theta = 90°$ than at $\theta = 30°$.

The emission at higher reduced frequencies appears to be more complicated.

The variation of $\phi(S)$ with jet diameter, that is Reynolds number, is very apparent. This is not due to variations in stagnation temperature, for example. Rather, the dependence of $\phi(S)$ upon Reynolds number seems to involve where transition from laminar to turbulent flow takes place. Because of the low turbulence level in the air supply, the boundary layer on the nozzle walls was laminar for the smaller diameter ($D = \frac{1}{2}$ in.) nozzle. Thus, transition took place in the free shear layer.

For the larger nozzle, transition took place in the boundary layer on the nozzle wall, but intermittently. An intermittent process involving very high local time derivatives may be a very efficient sound emitter.

For the largest jet diameter, $D = 1\frac{1}{2}$ in., the boundary layer on the nozzle wall was most likely fully turbulent. (No observations were made of the exit flow for this particular nozzle.) Preliminary measurements of the noise field from this larger nozzle indicate that the dependence of $\phi(S)$ upon Re changes from typically $\phi(S) \sim Re^2$ in the transitional range to $\phi(S) \sim Re$ when the boundary layer at the nozzle exit is fully turbulent. The length of the laminar core of the jet also varies with Reynolds number, and will also influence the effectiveness of the jet as a sound emitter. The data which show the details of the flow in the near field and within the jet will be published in a later paper.

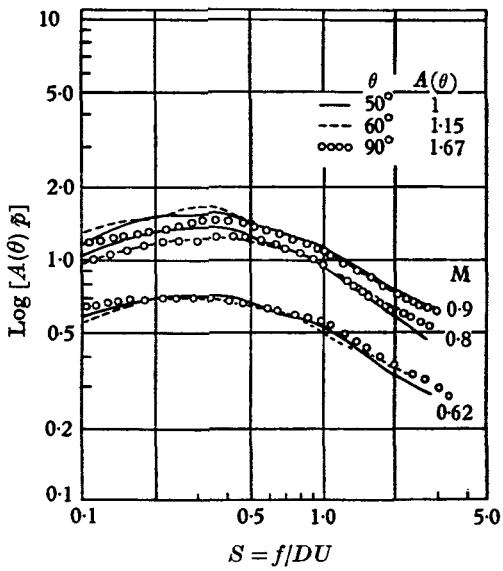

FIGURE 17. Similarity of spectra in directions well away from the jet axis.

Figure 17 shows that it may be possible to present the far field well away from the jet axis as a universal function of reduced frequency S times a function of M and θ only.

Figure 18 shows that such a simple approximation is not possible for θ less than 40°, but the figure suggests that for constant values of functional combinations of M and θ, the dependence upon reduced frequency S may be the same, so that $\phi(S, M, Re, \theta)$ has the form

$$\phi(S) = F\{f(M, \theta), S, Re\}.$$

This suggests that the effect of convection of sound emitters and sound by the mean flow of the jet is most strongly felt in the far field near the jet axis, a conclusion which is eminently reasonable, if not trivial. One fact is however interesting. We were unable to find any upstream intensity lobes, i.e. maxima of intensity for $90° < \theta < 180°$. This is in direct disagreement with previous experiments

(Fitzpatrick 1952; Lassiter 1952; Merle 1957; Franken 1958; Gerrard 1956) and with Lighthill's predictions (Lighthill 1954).

We could have obtained such upstream intensity lobes by letting the jet impinge on a solid object, or by mounting a sound reflector somewhere in the downstream sound field. This would, however, be a different experiment, perhaps already performed inadvertently by others.

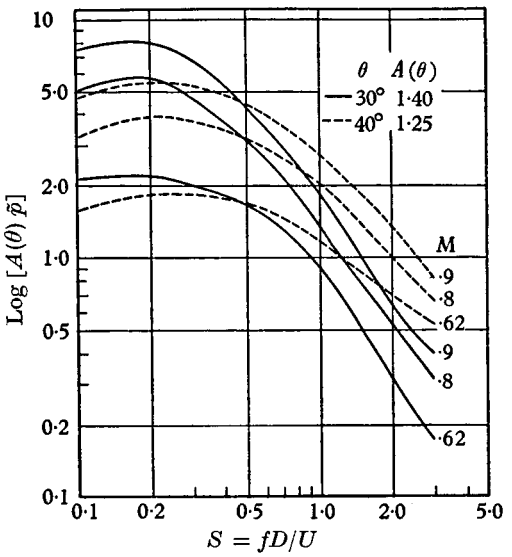

FIGURE 18. Similarity in spectra near the jet axis.

6. Conclusions

The results of the present measurements show no important discrepancies with previously obtained data, although some of the more tenuous conclusions drawn on the basis of previous data may be questioned.

There appear to be at least two distinguishable types of emitted sound, one dominating at very low frequencies and another dominating at high frequencies. A relation which gives a smooth interpolation between these asymptotic ranges would prove useful, if one could be invented.

The emitted sound depends upon the structure of the boundary layer at the nozzle exit, more strongly so when the boundary layer is not fully turbulent or very thin. This is supported by previous experiments (Mollo-Christensen & Narasimha 1960).

The process of generation of turbulence may determine the structure of the sound field two ways: directly, by sound emission from the transition process in the jet, and indirectly, by sound emitted from the turbulence convected downstream.

The near-field pressure covariances give an indication of this, and will be reported in a later paper. The length of the mixing region of a jet also affects sound emission, being itself dependent upon the efflux boundary layer.

These data suggest that some slight modifications of current thinking on the

subject of jet noise may be necessary. This will be further illustrated by the results of near-field and turbulence measurements, which will be reported in future papers.

This work was supported by the National Aeronautics and Space Administration under Grant NsG 31-60. The able assistance of Mr Fred Merlis in building, maintaining and keeping watch on the electronic equipment contributed significantly to the results.

REFERENCES

FITZPATRICK, H. M. & LEE, R. 1952 Measurements of noise radiated by subsonic air jets. *David Taylor Model Basin, Rep.* no. 83, Regular Ser.

FRANKEN, P. A. 1958 Review of information on jet noise. *Noise Control*, **4**, 8–16.

GERRARD, J. H. 1956 An investigation of the noise produced by a subsonic air jet. *J. Aero. Sci.* **23**, 855–66.

KOLPIN, M. A. 1962 Flow in the mixing region of a jet. *Mass. Inst. Tech. Aero-Sci. Res. Lab. Tech. Rep.* no. 92–3.

LASSITER, L. W. & HUBBARD, H. H. 1952 Experimental studies of noise from subsonic jets in still air. *Nat. Adv. Comm. Aero., Wash., Tech. Note*, no. 2757.

LIGHTHILL, M. J. 1954 On sound generated aerodynamically. II. *Proc. Roy. Soc.* A, **222**, 1–32.

LIGHTHILL, M. J. 1961 Sound generated aerodynamically; the Bakerian Lecture. *Royal Aircraft Establishment Tech. Memo.* Dir. 8.

MERLE, M. 1957 Nouvelles recherches sur la structure des jets à grande vitesse et les fréquences ultrasonores emises. *J. Phys. Radium*, **18**, 665–95.

MOLLO-CHRISTENSEN, E. & NARASIMHA, R. 1960 Sound emission from jets of high subsonic velocities. *J. Fluid Mech.* **8**, 49–60.

PRINTED IN GREAT BRITAIN AT THE UNIVERSITY PRINTING HOUSE, CAMBRIDGE
(BROOKE CRUTCHLEY, UNIVERSITY PRINTER)